Structure, Vol. 11, 147–154, February, 2003, ©2003 Elsevier Science Ltd. All rights reserved. PII S0969-2126(03)00004-2

Catalysis, Specificity, and ACP Docking Site of *Streptomyces coelicolor* Malonyl-CoA:ACP Transacylase

Adrian T. Keatinge-Clay,[1] Anang A. Shelat,[2] David F. Savage,[1] Shiou-Chuan Tsai,[3,4] Larry J.W. Miercke,[3] Joseph D. O'Connell III,[3] Chaitan Khosla,[4] and Robert M. Stroud[3,*]

[1]Graduate Group in Biophysics

[2]Graduate Group in Chemistry and Chemical Biology

[3]Department of Biochemistry and Biophysics
University of California, San Francisco
San Francisco, California 94143

[4]Departments of Chemistry, Chemical Engineering, and Biochemistry
Stanford University
Stanford, California 94305

Summary

Malonyl-CoA:ACP transacylase (MAT), the *fabD* gene product of *Streptomyces coelicolor* A3(2), participates in both fatty acid and polyketide synthesis pathways, transferring malonyl groups that are used as extender units in chain growth from malonyl-CoA to pathway-specific acyl carrier proteins (ACPs). Here, the 2.0 Å structure reveals an invariant arginine bound to an acetate that mimics the malonyl carboxylate and helps define the extender unit binding site. Catalysis may only occur when the oxyanion hole is formed through substrate binding, preventing hydrolysis of the acyl-enzyme intermediate. Macromolecular docking simulations with actinorhodin ACP suggest that the majority of the ACP docking surface is formed by a helical flap. These results should help to engineer polyketide synthases (PKSs) that produce novel polyketides.

Introduction

Polyketides are a diverse set of natural products including many pharmaceutically important agents such as erythromycin, tetracycline, and doxorubicin [1]. These secondary metabolites are produced by polyketide synthases (PKSs) found in many terrestrial and marine microorganisms as well as some plants. With the exception of plant PKSs, these biosynthetic complexes are organized as either a covalent (type I) or noncovalent (type II) assembly of catalytic domains, including at least one set of three core enzymes: a β-ketoacyl synthase (KS), an acyltransferase (AT), and an acyl carrier protein (ACP) [2, 3]. In some cases, an enzyme is shared by two or more related pathways [4, 5]. For example, *S. coelicolor* MAT serves as the AT in fatty acid and polyketide synthesis, providing extender units that are integrated into fatty acids, the *whiE* spore pigment, and the well-characterized antibiotic, actinorhodin [6].

The transfer reaction catalyzed by ATs resembles the serine protease mechanism. In the first half-reaction, a catalytic serine attacks the thioester carbonyl of an appropriate acyl-coenzyme A (malonyl-CoA in MAT), freeing CoA and forming an acyl-enzyme. Subsequently, the thiol of the ACP phosphopantetheine arm (approximately 18 Å long) attacks the ester carbonyl, yielding an acyl-ACP product. Because this product is then fused by a KS to the backbone of a growing carbon chain, it is the AT that acts as the primary gatekeeper for building blocks used during biosynthesis.

The structure of *Escherichia coli* MAT from the fatty acid biosynthesis pathway has been reported; however, the structural details of substrate binding and extender unit specificity were not apparent [7]. Here we report the structure of *S. coelicolor* MAT solved to 2.0 Å with an acetate anion bound in the active site. The reaction mechanism and specificity of ATs are discussed based on the bound acetate, and new models for acyl-CoA binding and ACP docking are presented.

Results and Discussion

Overall Structure

MAT is a 32 kDa monomer composed of two subdomains (Figure 1A). The large subdomain (residues 1–132 and 198–316) has a central parallel β sheet surrounded by 12 α helices, five of which form a helical flap on the protein surface. The core of this subdomain is structurally similar to α/β hydrolases. The small subdomain (residues 133–197) has a ferredoxin-like fold, with a four-stranded antiparallel β sheet and two α helices, observed in acylphosphatases as well as domains that bind metal, RNA, DNA, and protein [8, 9]. Perhaps MAT is best described as a distant relative of the α/β hydrolase superfamily, possessing a hydrolase core with insertions of a helical flap and a ferredoxin-like subdomain [10].

The overall structure of MAT from *S. coelicolor* is similar to that of its *E. coli* ortholog. The relative insertion of residues 79–86, absent in the electron density maps, does not alter the neighboring tertiary structure. The biggest structural differences are the extension of α7 by one turn, the shortening of α9 by one turn, and the extension of the C-terminal α14 by two turns. Interestingly, *S. coelicolor* MAT is slightly more compact. The two subdomains, linked to each other via two loops, appear to clasp the acetate using a slight hinge motion. The Cαs of highly conserved residues Gly10, from the large subdomain, and Leu194, from the small subdomain, are 1.5 Å closer than in the *E. coli* structure (10.2 Å).

Two acetate molecules from the crystallization buffer are bound to MAT (Figure 2). ACY 1 is bound to Gln9 and Arg122 in the active site and probably mimics the carboxyl end of a bound malonyl group. The arginine guanidino group and the acetate carboxylate are coplanar but rotated 30 degrees away from forming a bidentate salt bridge. ACY 2 stacks against the imidazole ring

*Correspondence: stroud@msg.ucsf.edu

Key words: polyketide synthase; actinorhodin; malonyl-CoA:ACP transacylase; acyltransferase; acyl carrier protein; macromolecular docking

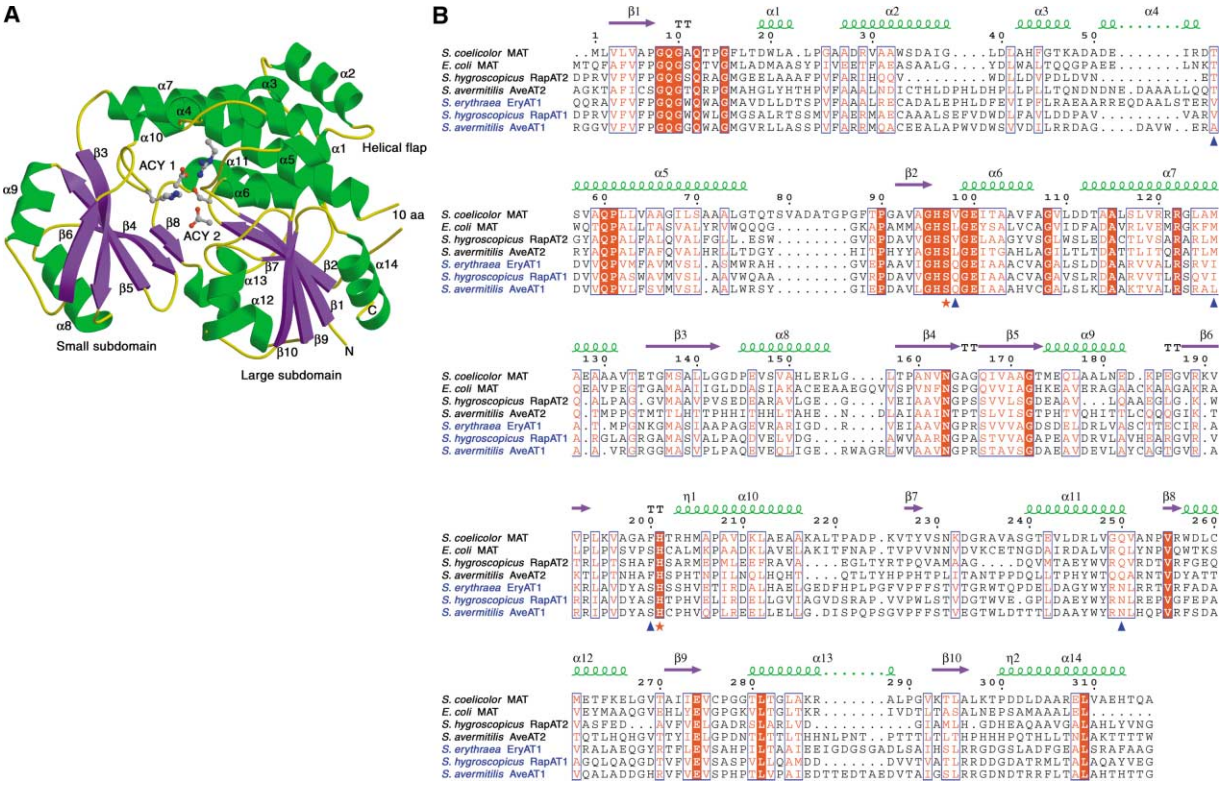

Figure 1. Structure of *S. coelicolor* MAT with Sequence Alignment

(A) The smaller ferredoxin-like subdomain is on the left (α8-9 and β3–6). A helical flap (α1–5 and β1) may be important in ACP docking. Conserved residues Ser97, Arg122, and His201, as well as both acetates, ACY 1 and ACY 2, are shown in ball and stick representation.

(B) Sequence alignment of malonyl-specific and methylmalonyl-specific ATs (names in black and blue, respectively). The last five ATs are from type I PKSs that participate in the synthesis of rapamycin (Rap), avermectin (Ave), and erythromycin (Ery). Strictly conserved and similar residues are surrounded by red and colored red, respectively. Catalytic residues are marked by stars. Residues important in substrate specificity are indicated by triangles. The alignment was made with ESPript.

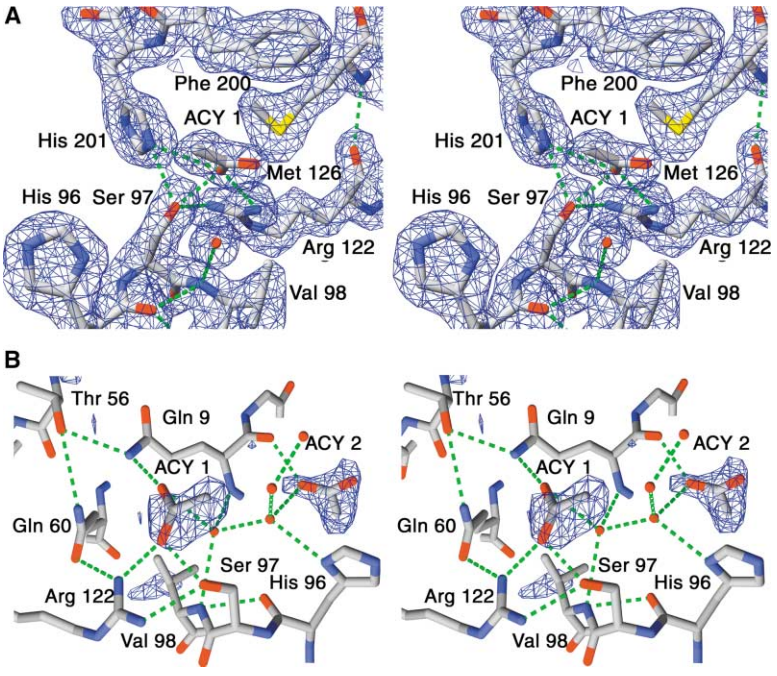

Figure 2. Electron Density Maps of the Active Site

(A) The $2F_o - F_c$ map contoured at 1.2 σ. His201 and Ser97 form the catalytic dyad. The carboxylate of ACY 1 is bound to the invariant residues Gln9 and Arg122. ACY 1 and a water molecule suggest where the malonyl group binds. Met126 and Phe200 probably form a selectivity filter that rejects α-substituted malonyl groups.

(B) Omit map of ACY 1 and ACY 2 contoured at 3.5 σ.

of His96 and hydrogen bonds to the backbone carbonyl of Gln9. The mean temperature factors for ACY 1 and ACY 2 (47 Å^2 and 37 Å^2, respectively) are slightly higher than that of the overall protein (33 Å^2). A crystal contact is mediated by what is likely a nickel ion from the purification, as judged by the difference map, tetrahedral coordination, and bond lengths to its ligands (three aspartates and one water). Both regions bound to it are more than 25 Å from the active site and unperturbed relative to *E. coli* MAT.

Catalysis

MAT catalyzes malonyl transfer via a ping-pong bi-bi mechanism using a His-Ser catalytic dyad [11]. The catalytic Ser97 lies at a nucleophilic elbow in a highly conserved GHSXG motif. Proton transfer occurs via His201, which is stabilized in an unusual manner through the backbone carbonyls of Gln250 and Asn253, instead of an aspartic or glutamic acid side chain customary in α/β hydrolases.

In the *E. coli* MAT structure, two plausible sites for the oxyanion hole are occupied by water molecules—one adjacent to two backbone amides and the other next to side chains of residues equivalent to Gln9 and Arg122 [7]. Because ACY 1 in our structure replaces the water contacting these side chains, it is likely that the backbone amides of Gln9 and Val98 create the oxyanion hole. Further support comes from Gln9 being structurally (primary, secondary, and tertiary) analogous to the residue whose amide helps stabilize the oxyanion in α/β hydrolases. The nitrogens of these amides are spaced 1.1 Å farther apart than in an average oxyanion hole (5.5 Å versus 4.4 Å); however, it is likely that upon substrate binding, the Gln9 amide is pushed toward the Val98 amide and a functional oxyanion hole is formed. This mechanism is used by members of the α/β hydrolase superfamily including some lipases that, upon the binding of substrate to a helical extrusion, undergo a transition from a "closed" to an "open" conformation in which the oxyanion hole has been assembled. Both Gln9 and the analogous lipase residue lie at the second position of highly conserved motifs (GQGXQ in ATs, G(M/L/V)XG in bacterial lipase families I.1 and I.2) and correspond structurally to the elbows of homologous turns [12, 13].

The first half-reaction catalyzed by MAT commences when malonyl-CoA binds to the enzyme (Figure 3A). The malonyl carboxylate presumably adopts a similar orientation to ACY 1, and the thioester carbonyl inserts into the oxyanion hole. In this configuration, the thioester plane is nearly perpendicular to that of the carboxylate. This is in contrast to a recently proposed model in which these groups are coplanar and the thioester carbonyl interacts with His96 instead of the oxyanion hole [14]. After malonyl-CoA is bound, Ser97 attacks the thioester carbonyl, forming a tetrahedral intermediate stabilized through a favorable charge-dipole interaction in the oxyanion hole. His201 subsequently protonates CoA, liberating it from malonyl-MAT. In order to accommodate the covalently bound malonyl group, the side chain of Arg122 must be displaced toward α7. In both *S. coelicolor* and *E. coli* MATs, there is room for the arginine to move in such a way. In the second half-reaction, ACP docks on the surface of malonyl-MAT, and the phosphopantetheinyl thiol enters the active site. Attack at the ester carbonyl is made possible through the assembly of the oxyanion hole, and another tetrahedral intermediate is formed. His201 then reprotonates the catalytic serine, eliminating malonyl-ACP.

We have tested mutations to active site residues, including Ser97 and His201 [15]. While the His201 → Ala mutant has no detectable catalytic activity, the Ser97 → Ala mutant has a k_{cat} only 10-fold lower than the native enzyme. Mass spectrometry analysis of this mutant shows His96 to be malonated, indicating that it may be a surrogate nucleophile. However, another study on the Ser97 → Ala mutant reported that it is incapable of malonyl transfer [16]. While ACY 2 is close to His96, it is in an incorrect orientation to be mimicking a bound malonyl group, and while the histidine is activated by the side chain of Asn163, nucleophilic attack would need to occur without the assistance of the described oxyanion hole. In any case, His96 is not critical to the reaction catalyzed by the native enzyme, as several known ATs have a leucine at this position and the His96 → Ala mutant is catalytically active [15].

Selectivity

While the selectivity of type II ATs is limited to malonyl extender units, the selectivity of type I ATs is wide ranging: loading ATs choose primer units such as acetyl-CoA, propionyl-CoA, or isobutyryl-CoA, while downstream ATs choose extender units such as malonyl-CoA, methylmalonyl-CoA, or ethylmalonyl-CoA. If the domain architectures between type I and type II ATs differ, it is not apparent how, by sequence alignment. Thus, while an AT domain in a type I PKS must experience some physical constraints by virtue of being linked to other enzymatic domains, it probably uses the same architectural features as a type II AT for selectivity. Indeed, malonyl-specific ATs from both type I and type II PKSs possess an equivalent set of what may be specificity-conferring residues. The identities of these residues are consistently different in methylmalonyl-specific ATs (Figure 1B).

Even though AT specificity can be predicted either for malonyl or α-substituted malonyl groups through sequence information alone [17, 18], no experiment has been successful in switching AT specificity. The crystal structure of *S. coelicolor* MAT with acetate bound therefore provides a new opportunity to define the precise structural basis for AT specificity.

The *S. coelicolor* MAT structure reveals that 2 residues, Met126 and Phe200, probably form the selectivity filter that acts against α substituents (Figure 3B). The inability of MAT to accept (2S)-methylmalonyl-CoA is explained by the methyl group sterically clashing with Phe200. Some MATs, such as the one from *E. coli*, have a serine in this position and are still selective for malonyl groups. The remaining methionine may prevent inappropriate acyl-enzyme formation by sterically interfering with α substituents at the tetrahedral intermediate stage. Alternatively, an effective filter can be formed by a lone

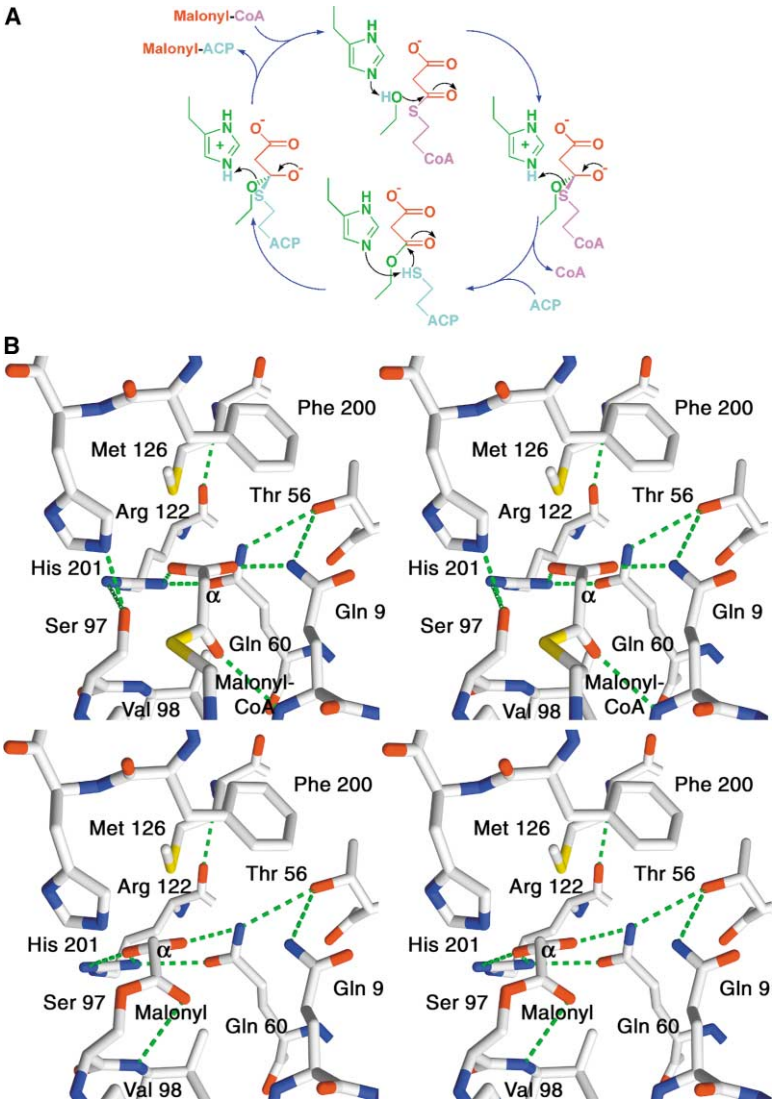

Figure 3. MAT Transfers a Malonyl Group from Malonyl-CoA to ACP

(A) In the first half-reaction, the catalytic serine attacks a bound malonyl-CoA at the thioester carbonyl, forming a tetrahedral intermediate that collapses to release CoA from malonyl-MAT. In the second half-reaction, the malonyl-MAT ester carbonyl is attacked by the phosphopantetheinyl thiol of ACP, forming a second tetrahedral intermediate that collapses to yield malonyl-ACP.

(B) The top and bottom stereograms show models of malonyl-CoA-bound MAT and malonyl-MAT, respectively. A substrate with a substituent projecting from the α carbon (S stereochemistry being to the right) would be rejected by a selectivity filter formed by Phe200 and Met126. The backbone amide of Gln9 may move closer to the Val98 amide upon malonyl-CoA binding or ACP docking.

phenylalanine, as in a rapamycin PKS AT (module 14). Thus, although a majority of MATs possess both residues, it appears that only one of the 2 residues is required for specificity toward the malonyl group.

Other ATs are selective toward methylmalonyl-CoA, ethylmalonyl-CoA, or even methoxymalonyl-CoA. Residues consistently different between these ATs and malonyl-specific ATs are likely to influence substrate specificity. In particular, the residue after the catalytic serine is a branched hydrophobic amino acid in malonyl-specific ATs (Val98 in the *S. coelicolor* enzyme) and a glutamine in all other ATs. A threonine (Thr56) in malonyl-specific ATs forms a hydrogen bond with the NH_2 of a highly conserved glutamine (Gln9), while other ATs have a valine or alanine in this position. Without this hydrogen bond, the highly conserved glutamine (Gln9) of α substituent-accepting ATs may bond to the glutamine after the catalytic serine, opening up a hydrophobic environment for α substituents. This environment is further enlarged as Met126 and Phe200 are replaced by smaller amino acids.

The specificities of AT domains have been altered through regional swapping and through mutagenesis. A relaxed AT that accepts both malonyl-CoA and methylmalonyl-CoA was engineered by swapping a C-terminal segment (α13-14 and β10) from a malonyl-specific AT into a methylmalonyl-specific AT [19]. Swapping entire AT domains has often led to a loss in the catalytic abilities of a PKS, possibly due to nonnative interactions with the rest of the PKS. In the erythromycin PKS, only one AT (module 4) cannot be swapped out. In an effort to make this AT malonyl specific, three regions, including 3 of the 5 residues identified in Figure 1B, were altered by site-directed mutagenesis, both individually and in tandem [14]. The engineered ATs were shown to accept both malonyl and methylmalonyl groups, with the tandem mutant possessing the highest selectivity for malonyl groups at 50%. Combinatorial mutagenesis of the cited 5 residues will provide a valuable test of our substrate specificity model and may introduce a superior alternative to domain swapping in engineering novel polyketides.

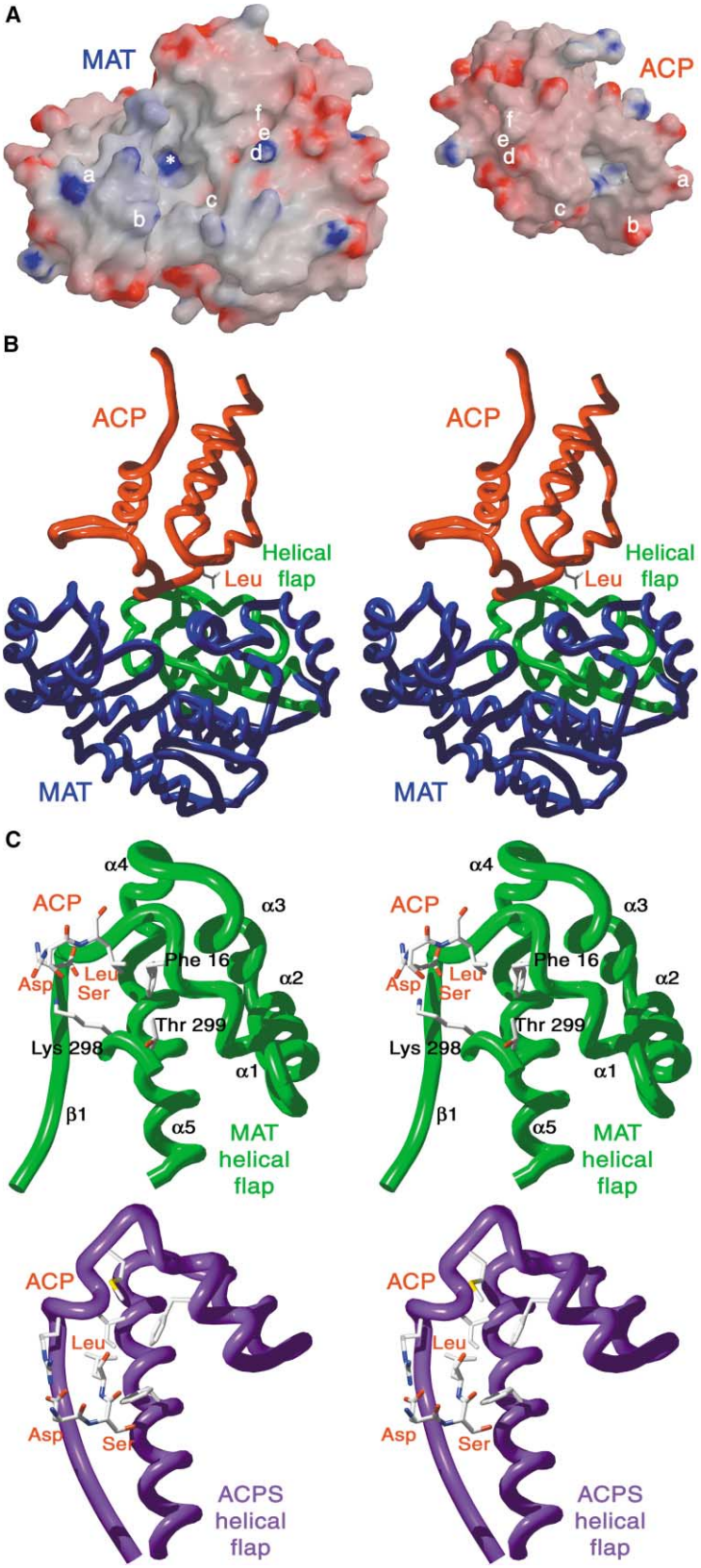

Figure 4. ACP Docked to MAT around the Helical Flap Region

(A) GRASP surfaces of *S. coelicolor* MAT and actinorhodin apo-ACP are represented so that if ACP were rotated by 180° on top of MAT, the same letter from each surface would match up. On ACP: a = Asp22, b = Asp25, c = α2, d = Asp41, e = Ser42, f = Leu43. Holo-ACP possesses a phosphopantetheine arm attached to Ser42 that might follow a surface groove to the active site (*), approximately 20 Å away.

(B) Lowest energy docking model between MAT and ACP. The highly conserved leucine of ACP inserts into a hydrophobic pocket created by the helical flap.

(C) The Asp-Ser-Leu motif of ACP binds to the helical flap region of MAT (from the docking model) and ACPS (from the ACP/ACPS complex structure, without the phosphopantetheine arm). The helical flaps formed by the N-terminal 64 residues of ACPS and the N-terminal 75 residues of MAT (together with Lys298 and Thr299) create similar hydrophobic pockets.

ACP Docking Site

In order for acyl transfer to occur specifically between an AT and an ACP, it is likely that they recognize one another. Given the constraints of the buried AT active site and the length of the phosphopantetheine arm, an ACP docking site may be present on the AT surface. In type II PKSs, there is evidence that ACP docking sites are also present on the KS and other PKS enzymes [20]. While type I ACPs are tethered by peptide to other enzymes in the PKS, it is conceivable that these linkages are flexible, allowing the ACP to dock to the appropriate modular enzymes, although there is little architectural data on the type I PKSs that can speak to this proposed flexibility.

The interface between ACP and MAT may be similar to that between apo-ACP and the phosphopantetheinyl transferase ACPS, which converts apo-ACP into holo-ACP [21]. The phosphopantetheine arm is attached to a serine located at the N-terminal end of the ACP α3 in a highly conserved Asp-Ser-Leu motif. In the ACPS/ACP crystal structure, residues in and surrounding the Asp-Ser-Leu motif are important for docking; the leucine and other hydrophobic residues on the same side of α3 insert into hydrophobic pockets on the ACPS, and the aspartate forms a salt bridge with a conserved arginine. Peripheral hydrophilic contacts may also be important in binding. A structural motif in ACPS (N-terminal 64 residues; originally observed in another phosphopantetheinyl transferase, Sfp [22]) that makes most of the contacts with ACP resembles the helical flap of MAT (N-terminal 75 residues). Electrostatic potential surfaces indicate that the Asp-Ser-Leu motif of ACP is complementary to a pocket on MAT formed by this flap (Figure 4A).

To analyze this potential interface in greater detail, we performed macromolecular docking experiments with unliganded MAT and actinorhodin apo-ACP. The lowest energy model indeed places the leucine into a hydrophobic pocket formed by the helical flap (Figure 4B). One of the major hydrophobic contacts made by the leucine is to a large hydrophobic residue in the helical flap (Phe16 in *S. coelicolor* MAT and methionine in nearly all other ATs; Figure 4C). The pocket lies immediately adjacent to the GQGXQ turn containing the oxyanion hole-forming Gln9. The helix that helps form the analogous turn of ACPS partially unwinds through the binding of ACP. Presumably, ACP docking to MAT causes Gln9 to be pushed toward the active site, creating a functional oxyanion hole. This mechanism allows the phosphopantetheine thiol of a docked ACP to react with malonyl-MAT while preventing the hydrolysis of malonyl-MAT in the absence of ACP. The invariant ACP serine is positioned approximately 20 Å from the catalytic serine of MAT, a distance that can be spanned by the phosphopantetheine arm via a groove on the surface of MAT. Along this groove lies the invariant Asn163 that is hydrogen bonded to the highly conserved His96 such that its side chain NH_2 is appropriately positioned to hydrogen bond to a carbonyl of the extended phosphopantetheine arm. The model also reveals a salt bridge between the conserved aspartate of ACP and Lys298. In the *E. coli* MAT, the analogous positive charge comes from a lysine that replaces Gly279. Most ATs have a positively charged residue at one of these two positions.

Our model provides new theories for how MAT interacts with its substrates. It has been proposed that the ferredoxin-like subdomain of MAT provides the major ACP docking surface [8, 20]. While our model shows some contact in this region, most of the interface lies on the large subdomain around the helical flap. The binding of an acyl-CoA may be similar to ACP docking, with its phosphopantetheine arm following the same groove, a phosphate moiety salt bridging to Lys298, and the adenine binding in the hydrophobic pocket. If mutational analysis of interfacial residues both on MAT and ACP supports the docking model, ATs and ACPs could be engineered for compatibility in hybrid PKSs designed to produce novel polyketides.

Biological Implications

In *S. coelicolor*, MAT is a key enzyme in both fatty acid and polyketide synthesis. The well-characterized polyketide antibiotic actinorhodin is synthesized entirely from the malonyl groups that it selects. Because of its homology to ATs that are present in every PKS, an understanding of the mechanism and selectivity of MAT is invaluable in designing PKSs capable of synthesizing novel polyketides, antibiotics included.

The assembly line nature of type I PKSs, in which ATs select extender units to be added at particular stages of chain growth, has allowed the synthesis of novel polyketides through swapping in heterologous AT domains possessing other specificities. However, possibly due to nonnative interactions, domain swapping often causes decreased fidelity and processivity, resulting in lower polyketide titers. The structure of *S. coelicolor* MAT bound to acetate suggests how an AT can be selective for malonyl extender units and possibly how homologous ATs can select α-substituted extender units. Thus, it may be possible to use site-directed mutagenesis to change AT specificity while keeping the PKS intact, allowing the production of a combinatorial number of novel polyketides.

If the interactions that AT makes with the rest of the PKS were better understood, domain swapping could become more reliable. ATs probably cooperate most closely with their substrate ACPs. From the electrostatic surfaces, conserved structural motifs, and docking simulations of *S. coelicolor* MAT and actinorhodin ACP, it appears they associate via a hydrophobic pocket on the surface of MAT. This docking would allow the phosphopantetheine arm of ACP to access the malonyl group bound to MAT. The malonated ACP could then dissociate, passing the extender unit on to be integrated into a complex molecule.

It should be remembered that MAT is also representative of AT domains in fatty acid synthases, because PKSs and fatty acid synthases are evolutionarily related. Somewhat ironically, fatty acid synthases have historically been targets of antibiotics.

Experimental Procedures

Expression, Purification, and Crystallization

MAT was expressed from *E. coli* strain BL21 (Novagen) transformed with a pET28a vector (Novagen) with the *S. coelicolor fabD* gene

Table 1. Crystallization Data and Refinement Statistics

Crystallization	
Space group	$P2_12_12_1$
Unit cell (Å)	a, b, c = 43.1, 54.5, 109.9
Wavelength (Å)	1.127
Resolution (Å)	2.0
Unique reflections	17,011
Total reflections	65,258
Completeness (%)[a]	93.7 (85.6)
R_{sym}[a]	8.1 (41.2)
$<I/\sigma(I)>$[a]	6.2 (1.7)
Refinement	
R_{cryst}	19.7
R_{free}[b]	23.2
Rmsd	
Bond (Å)	0.005
Angle (°)	1.2
Number of atoms	
Protein	2,183
Water	108
Acetate	8
Nickel	1
Mean B factors (Å^2)	
Protein	32.5
Water	22.2
Acetate	41.5
Nickel	28.9

[a] Number in parentheses is for the last shell.
[b] R_{free} was calculated on 10% of data excluded before refinement.

inserted between the NdeI and EcoRI restriction sites (plasmid GFL17 from G. Liou, personal communication). Bacteria were induced at 1 mM IPTG for 3 hr. After pelleting, cells were resuspended in 0.5 M NaCl, 10 mM Tris-HCl (pH 7.4), 1 mM β-ME, and 0.1 mM PMSF, and sonicated. The lysed cells were spun down at 45,000 × g, and the lysate was poured over a nickel-NTA column (Qiagen). MAT eluted at 50 mM imidazole and was greater than 99% pure, as estimated by SDS-PAGE followed by Coomassie staining. The protein was dialyzed into 10 mM Tris-HCl (pH 7.4) and 1 mM β-ME and concentrated to 3 mg ml^{-1}. Crystals grew to 50 × 50 × 150 μm in 3 days by hanging drop vapor diffusion at room temperature using 25% PEG4000, 100 mM sodium acetate (pH 4.8), and 200 mM ammonium acetate.

Data Collection and Structure Determination

Crystals were soaked in 30% PEG4000, 100 mM sodium acetate (pH 4.8), 200 mM ammonium acetate, and 20% glycerol before cooling in a nitrogen stream. X-ray data were collected at ALS beamline 8.3.1 (λ = 1.127 Å). Diffraction images were autoindexed and integrated with MOSFLM [23] and then scaled and merged with SCALA [24]. The structure was solved by molecular replacement using CNS [25] with the *E. coli* MAT (PDB code 1MLA) as a search model. Building and refinement were performed with QUANTA (Accelrys) and CNS, respectively. CNS topology and parameter files for acetate were obtained from HIC-up [26]. The model contains 303 residues from MAT (residues 1–76 and 87–314), one His_6 tag residue, 108 waters, and one nickel atom (Table 1). Figures were prepared with MOLSCRIPT [27], RASTER3D [28], Swiss-PdbViewer [29], POV-Ray [30], and GRASP [31].

Macromolecular Docking

Rigid docking of actinorhodin ACP (PDB code 2AF8) and MAT was performed using the DOCK 4.0 program suite [32]. To exhaustively search the binding surface of MAT, two sphere sets were generated covering the large and the small subdomains. One docking experiment was performed with each sphere set. The minimum number of nodes allowed in a clique was five, with a maximum of ten million orientations allowed for each sphere set. Orientations were rapidly scored using an energy grid with a 6-9 attractive-repulsive van der Waals potential and the electrostatic term weighted by 0.01. The energy minimization option was activated with default values. A bump filter was employed to discard orientations with greater than 100 major steric clashes. Residues Lys47, Lys190, Arg287, and Lys293 were mutated to alanine prior to docking, as their side chains had high B factors; these side chains were added back for all subsequent steps. The top ten scoring ligand orientations resulting from each dock run were minimized using the generalized Born/surface area (GB/SA) option in the AMBER 7.0 [33] Sander module (*igb* = 1, *saltcon* = 0.2 M, *gbsa* = 1) based on the following protocol: 500 steps steepest descent (SD) minimization with a 5000 kcal mol^{-1} restraint on all heavy atoms, followed by five rounds of 500 steps of SD minimization with 25, 20, 15, 10, and 5 kcal mol^{-1} restraints on all atoms, then 5000 steps of SD minimization with no restraints. The top five orientations scored similarly, and were subjected to further refinement with molecular dynamics in Sander using the GB/SA options previously described and a 20 kcal mol^{-1} restraint on backbone heavy atoms. The complex was heated from 10 K to 300 K over 10 ps, followed by equilibration at 300 K for 15 ps. The resulting structures were then subjected to 2000 steps of SD minimization. The best orientation, significantly lower in energy than the other orientations, is described.

Acknowledgments

We thank Grace Liou for supplying the GFL17 plasmid, James Holton for helping collect and process the diffraction data, Irwin Kuntz for access to the computer resources for the docking calculations, as well as Tom Lee, Pascal Egea, and Julian Chen for their advice. A.T.K.-C. was supported by NIH Cancer Institute grants CA 63081 (R.M.S.) and CA 77248 (C.K.) as well as by NIH grant NIGMS T32 08284. A.A.S. was supported by a fellowship from the National Defense Science and Engineering Graduate Program.

Received: August 6, 2002
Revised: November 12, 2002
Accepted: November 15, 2002

References

1. O'Hagan, D.O. (1991). The Polyketide Metabolites (Chichester, UK: Ellis Horwood).
2. Hopwood, D.A. (1997). Genetic contributions to understanding polyketide synthases. Chem. Rev. *97*, 2465–2498.
3. Cane, D.E., Walsh, C.T., and Khosla, C. (1998). Harnessing the biosynthetic code: combinations, permutations, and mutations. Science *282*, 63–68.
4. Revill, W.P., Bibb, M.J., and Hopwood, D.A. (1995). Purification of a malonyltransferase from *Streptomyces coelicolor* A3(2) and analysis of its genetic determinant. J. Bacteriol. *177*, 3946–3952.
5. Summers, R.G., Ali, A., Shen, B., Wessel, W.A., and Hutchinson, C.R. (1995). Malonyl-coenzyme A:acyl carrier protein acyltransferase of *Streptomyces glaucescens*: a possible link between fatty acid and polyketide biosynthesis. Biochemistry *34*, 9389–9402.
6. Carreras, C.W., and Khosla, C. (1998). Purification and in vitro reconstitution of the essential protein components of an aromatic polyketide synthase. Biochemistry *37*, 2084–2088.
7. Serre, L., Verbree, E.C., Dauter, Z., Stuitje, A.R., and Derewenda, Z.S. (1995). The *Escherichia coli* malonyl-CoA:acyl carrier protein transacylase at 1.5-Å resolution. Crystal structure of a fatty acid synthase component. J. Biol. Chem. *270*, 12961–12964.
8. Lo Conte, L., Brenner, S.E., Hubbard, T.J., Chothia, C., and Murzin, A.G. (2002). SCOP database in 2002: refinements accommodate structural genomics. Nucleic Acids Res. *30*, 264–267.
9. Welch, M., Chinardet, N., Mourey, L., Birck, C., and Samama, J.P. (1998). Structure of the CheY-binding domain of histidine kinase CheA in complex with CheY. Nat. Struct. Biol. *5*, 25–29.
10. Katz, L., and McDaniel, R. (1999). Novel macrolides through genetic engineering. Med. Res. Rev. *19*, 543–558.
11. Joshi, V.C., and Wakil, S.J. (1971). Studies on the mechanism of fatty acid synthesis. XXVI. Purification and properties of malo-

nyl-coenzyme A-acyl carrier protein transacylase of *Escherichia coli*. Arch. Biochem. Biophys. *143*, 493–505.
12. Roussel, A., Miled, N., Berti-Dupuis, L., Riviere, M., Spinelli, S., Berna, P., Gruber, V., Verger, R., and Cambillau, C. (2002). Crystal structure of the open form of dog gastric lipase in complex with a phosphonate inhibitor. J. Biol. Chem. *277*, 2266–2274.
13. Nardini, M., Lang, D.A., Liebeton, K., Jaeger, K.E., and Dijkstra, B.W. (2000). Crystal structure of *Pseudomonas aeruginosa* lipase in the open conformation. The prototype for family I.1 of bacterial lipases. J. Biol. Chem. *275*, 31219–31225.
14. Reeves, C.D., Murli, S., Ashley, G.W., Piagentini, M., Hutchinson, C.R., and McDaniel, R. (2001). Alteration of the substrate specificity of a modular polyketide synthase acyltransferase domain through site-specific mutations. Biochemistry *40*, 15464–15470.
15. Dreier, J., Li, Q., and Khosla, C. (2001). Malonyl-CoA:ACP transacylase from *Streptomyces coelicolor* has two alternative catalytically active nucleophiles. Biochemistry *40*, 12407–12411.
16. Szafranska, A.E., Hitchman, T.S., Cox, R.J., Crosby, J., and Simpson, T.J. (2002). Kinetic and mechanistic analysis of the malonyl CoA:ACP transacylase from *Streptomyces coelicolor* indicates a single catalytically competent serine nucleophile at the active site. Biochemistry *41*, 1421–1427.
17. Haydock, S.F., Aparicio, J.F., Molnar, I., Schwecke, T., Khaw, L.E., Konig, A., Marsden, A.F., Galloway, I.S., Staunton, J., and Leadlay, P.F. (1995). Divergent sequence motifs correlated with the substrate specificity of (methyl)malonyl-CoA:acyl carrier protein transacylase domains in modular polyketide synthases. FEBS Lett. *374*, 246–248.
18. Tang, L., Yoon, Y.J., Choi, C.Y., and Hutchinson, C.R. (1998). Characterization of the enzymatic domains in the modular polyketide synthase involved in rifamycin B biosynthesis by *Amycolatopsis mediterranei*. Gene *216*, 255–265.
19. Lau, J., Fu, H., Cane, D.E., and Khosla, C. (1999). Dissecting the role of acyltransferase domains of modular polyketide synthases in the choice and stereochemical fate of extender units. Biochemistry *38*, 1643–1651.
20. Zhang, Y.M., Rao, M.S., Heath, R.J., Price, A.C., Olson, A.J., Rock, C.O., and White, S.W. (2001). Identification and analysis of the acyl carrier protein (ACP) docking site on β-ketoacyl-ACP synthase III. J. Biol. Chem. *276*, 8231–8238.
21. Parris, K.D., Lin, L., Tam, A., Mathew, R., Hixon, J., Stahl, M., Fritz, C.C., Seehra, J., and Somers, W.S. (2000). Crystal structures of substrate binding to *Bacillus subtilis* holo-(acyl carrier protein) synthase reveal a novel trimeric arrangement of molecules resulting in three active sites. Structure *8*, 883–895.
22. Reuter, K., Mofid, M.R., Marahiel, M.A., and Ficner, R. (1999). Crystal structure of the surfactin synthetase-activating enzyme sfp: a prototype of the 4′-phosphopantetheinyl transferase superfamily. EMBO J. *18*, 6823–6831.
23. Leslie, A.G.W. (1994). MOSFLM Users Guide (Cambridge, UK: MRC-LMB).
24. CCP4 (Collaborative Computational Project 4) (1994). The CCP4 suite: programs for protein crystallography. Acta Crystallogr. D *50*, 760–763.
25. Brunger, A.T., Adams, P.D., Clore, G.M., DeLano, W.L., Gros, P., Grosse-Kunstleve, R.W., Jiang, J.S., Kuszewski, J., Nilges, M., Pannu, N.S., et al. (1998). Crystallography & NMR system: a new software suite for macromolecular structure determination. Acta Crystallogr. D *54*, 905–921.
26. Kleywegt, G.J., and Jones, T.A. (1998). Databases in protein crystallography. Acta Crystallogr. D *54*, 1119–1131.
27. Kraulis, P.J. (1991). MOLSCRIPT: a program to produce both detailed and schematic plots of protein structures. J. Appl. Crystallogr. *24*, 946–950.
28. Merritt, E.A., and Bacon, D.J. (1997). Raster3D photorealistic molecular graphics. Methods Enzymol. *277*, 505–524.
29. Guex, N., and Peitsch, M.C. (1997). SWISS-MODEL and the Swiss-PdbViewer: an environment for comparative protein modeling. Electrophoresis *18*, 2714–2723.
30. POV-Ray Team (2002). Persistence of Vision Ray-Tracer (version 3.5). Retrieved from http://www.povray.org/binaries/index.html.
31. Nicholls, A., Sharp, K.A., and Honig, B. (1991). Protein folding and association: insights from the interfacial and thermodynamic properties of hydrocarbons. Proteins *11*, 281–296.
32. Ewing, T.J.A., and Kuntz, I.D. (1997). Critical evaluation of search algorithms used in automated molecular docking. J. Comput. Chem. *18*, 1175–1189.
33. Case, D.A., Pearlman, J.W., Caldwell, T.E., Cheatham, J., III, Wang, W.S., Ross, C.L., Simmerling, T.A., Darden, K.M., Merz, R.V., Stanton, A.L., et al. (2002). AMBER 7 (San Francisco: University of California).

Accession Numbers

The coordinates for the MAT structure and the theoretical MAT-ACP structure have been deposited in the Protein Data Bank under ID codes 1NM2 and 1NNZ, respectively.